Slip velocity and velocity inversion in a cylindrical Couette flow

Sangrak Kim*
Department of Physics, Kyonggi University, 94-6 Eui-dong, Youngtong-ku, Suwon 440-760, Korea
(Received 2 November 2008; published 25 March 2009)

Velocity inversion in a nanoscale cylindrical Couette flow is investigated with the Navier-Stokes (NS) equation and molecular-dynamics (MD) simulation. With general slip boundary conditions in the NS equation, the flow can be classified into five distinct profiles. The condition of velocity inversion is explored in the whole space of four dimensionless variables of β, slip velocity ratio u', radius ratio a', and angular velocity ratio ω'. MD computer simulations are performed to estimate the constitutive coefficient of the slip velocities at the walls. The flow is generated by a rotating inner wall and a stationary outer wall in conformity with the theoretical result. By varying an attraction parameter in the Lennard-Jones potential, the slip velocities can be easily controlled. The theoretical predictions are compared with the simulation results. We find that in the intermediate range of the attraction parameter the two results are quite comparable to some extent, but at both extreme values of the attraction parameter, they are quite different.

DOI: 10.1103/PhysRevE.79.036312 PACS number(s): 47.61.−k, 02.70.Ns, 05.60.−k, 47.11.Mn

I. INTRODUCTION

Recently there is a great interest in understanding the fundamental physics of slip flow in nanoscales [1–3]. This is due to the strong need for new theoretical tools to accurately model nanoscale physical processes and design new nanodevices. The physics at a solid wall surface thus plays a critical role in nanofluidics [4,5] since the relative importance of the interaction between fluid particles and solid wall particles increases as the device size shrinks to nanoscale.

Cylindrical Couette flow between two concentric cylinders, which is one of the slip flows, is a well-known classical fluid-dynamics problem treated even in elementary fluid-dynamics textbooks [6]. However, recent analytical and/or simulation studies have reported that under certain conditions the flow between cylinders can show a rather unexpected behavior: velocity inversion [7–13]. In the case of a stationary outer wall and a rotating inner wall, for example, the velocity profile can be reversed with the tangential velocity increasing from the inner wall to the outer wall, contrary to intuition.

This phenomenon of velocity inversion was first noticed by Einzel *et al.* [7]. With their theoretical model, they predicted that the velocity profile would become inverted for larger slip lengths. Tibbs *et al.* [8] further extended the formulation to the rarefied gas system. They presented velocity profiles with different accommodation coefficients. This was further observed in a nanoscale system. Jung [13] simulated this phenomenon of velocity inversion using molecular-dynamics (MD) simulations and found that it is strongly related to the degree of slip velocities between the fluid and the outer wall.

Here we will more generally examine the phenomenon by combining the Navier-Stokes (NS) equation with MD simulation in order to understand the mechanism of velocity inversion. Yuhong *et al.* [11] extended Tibbs *et al.*'s [8] formulation but still assumed the rarefied gas system and Maxwell's boundary condition. We assume only general slip boundary conditions at both walls without adopting accommodation coefficient. MD simulations were performed to get the constitutive property of slip velocities at both walls and β defined in Eq. (6). Calculated slip velocities are easily controlled by the attraction parameter α in Eq. (16). We will first present some theoretical results of the NS equation for the cylindrical Couette flow to explore the condition of velocity inversion in the whole four-dimensional space. Next we present MD simulation results for estimating slip velocities by varying the attraction parameter. Finally, we will analyze these results to explain the phenomenon of velocity inversion.

II. THEORETICAL CONSIDERATION

Let us consider a fluid flow between two concentric cylinders with inner radius a_i and outer radius a_o, respectively. Let ω_i and ω_o be the steady angular velocities of inner and outer cylinders, respectively. Since the system has a cylindrical symmetry, we have only the tangential component of flow velocity u_θ and furthermore it is a function of r only:

$$\vec{u} = u_\theta(r)\,\hat{\theta}. \tag{1}$$

From the continuity equation and the NS equation, we get [6]

$$u_\theta(r) = Ar + \frac{B}{r}, \tag{2}$$

where A and B are constants of the integration to be determined from the imposed boundary conditions. Now the problem is how to fix the constants A and B. In most cases, the nonslip (or stick) boundary conditions are assumed:

$$u_\theta(a_i) = \omega_i a_i, \quad u_\theta(a_o) = \omega_o a_o. \tag{3}$$

The molecular interaction between fluid particles and solid-surface particles is modeled by a boundary condition in the macroscopic theoretical approach. Here let us generalize

*srkim@kgu.ac.kr

TABLE I. The four types of $u_\theta(r)$ in Eq. (2).

Type	Sign(A)	Sign(B)	Characteristics
T1	+	+	U-shaped
T2	+	−	Monotonically increasing
T3	−	+	Monotonically decreasing
T4	−	−	Inverted U-shaped

the boundary conditions to include velocity slips at the surface of the walls, and assume that the slip velocities u_i and u_o at inner and outer walls, respectively, are

$$u_\theta(a_i) = \omega_i a_i - u_i, \quad u_\theta(a_o) = \omega_o a_o - u_o. \tag{4}$$

Then the constants are determined

$$A = \frac{(\omega_o a_o^2 - \omega_i a_i^2) - (u_o a_o - u_i a_i)}{a_o^2 - a_i^2}, \tag{5a}$$

$$B = \frac{a_i a_o}{a_o^2 - a_i^2}\{(\omega_i - \omega_o) a_i a_o - (u_i a_o - u_o a_i)\}. \tag{5b}$$

If we set $u_i = u_o = 0$ in Eqs. (5), we get the usual form for nonslip boundary conditions given by Eq. (3):

$$A = \frac{(\omega_o a_o^2 - \omega_i a_i^2)}{a_o^2 - a_i^2}, \tag{6a}$$

$$B = \frac{a_i^2 a_o^2}{a_o^2 - a_i^2}(\omega_i - \omega_o). \tag{6b}$$

Equation (6) appears even in introductory fluid mechanics textbooks [6].

The functional form of $u_\theta(r)$ in Eq. (2) has an interesting property and can be classified into four types according to the signs of constants A and B, as in Table I. Type 2 (T2) has the property of $du_\theta(r)/dr > 0$ and type 3 (T3) $du_\theta(r)/dr < 0$. Type 1 (T1) has the property of $d^2u_\theta(r)/dr^2 > 0$ and type 4 (T4) $d^2u_\theta(r)/dr^2 < 0$. We can assume, without loss of generality, $\omega_i \omega_o \geq 0$, i.e., the same direction of rotation. Then T4 can be excluded from our considerations, without loss of generality.

We now express A and B in a dimensionless form by dividing ω_i and $\omega_i a_i^2$, respectively. Then we have

$$A' \equiv \frac{A}{w_i} = \frac{(\omega' a'^2 - 1) - \beta(u' a' - 1)}{a'^2 - 1}, \tag{7a}$$

$$B' \equiv \frac{B}{w_i a_i^2} = \frac{a'\{(1 - \omega')a' - \beta(a' - u')\}}{a'^2 - 1}, \tag{7b}$$

where $\beta = u_i/w_i a_i$, slip velocity ratio $u' = u_o/u_i$, radius ratio $a' = a_o/a_i$, and angular velocity ratio $\omega' = \omega_o/\omega_i$. Note that $a' > 1$. By setting $A' = 0$ and $B' = 0$ and solving them for ω' with β as a parameter, we get

$$\omega' = \beta u'/a' + (1 - \beta)/a'^2, \tag{8a}$$

$$\omega' = 1 - \beta + \beta u'/a'. \tag{8b}$$

Note that as $\beta \to 1$, Eq. (8a) becomes the same as Eq. (8b). If we differentiate Eq. (2), we get

$$\frac{du_\theta(r)}{dr} = A - \frac{B}{r^2}. \tag{9}$$

Since $a_i < r < a_o$, which actually is our interesting range of r, we have the inequalities

$$A - \frac{B}{a_i^2} < \frac{du_\theta(r)}{dr} < A - \frac{B}{a_o^2}. \tag{10}$$

We can thus consider three distinct cases, depending on the location satisfying $\frac{du_\theta(r)}{dr} = 0$: (1) $A - \frac{B}{a_i^2} \geq 0$, (2) $A - \frac{B}{a_o^2} \leq 0$, and (3) $A - \frac{B}{a_i^2} < 0$ and $A - \frac{B}{a_o^2} > 0$.

Case 1 (C1) implies $du_\theta(r)/dr \geq 0$, i.e., $u_\theta(r)$ monotonically increases for $a_i < r < a_o$. Case 2 (C2) implies $du_\theta(r)/dr \leq 0$, i.e., $u_\theta(r)$ monotonically decreases for $a_i < r < a_o$. Case 3 (C3) implies that there exists $\tilde{r}$ such that $\frac{du_\theta(r)}{dr}|_{r=\tilde{r}} = 0$ where $a_i < \tilde{r} < a_o$. Thus the velocity inversion occurs at $r = \tilde{r}$ for $a_i < \tilde{r} < a_o$.

Now let us examine these cases more clearly. Setting $A - \frac{B}{a_i^2} = 0$ and $A - \frac{B}{a_o^2} = 0$ and solving them for ω' with β as a parameter as before, we get

$$\omega' = \frac{1 - \beta}{2a'^2} + \beta\frac{u'}{a'} + \frac{1 - \beta}{2}, \tag{11a}$$

$$\omega' = \frac{\beta u' a' + 2(1 - \beta) + \beta\dfrac{u'}{a'}}{1 + a'^2}. \tag{11b}$$

Note that as $\beta \to 1$, Eq. (11a) also becomes the same as Eq. (11b).

To explore the types of u_θ and cases of du_θ/dr, we plot ω' defined by Eqs. (8) and (11) in a single graph. They are shown in Fig. 1. There are four surfaces. Thus the (a', u', ω') space is divided into five regions. The bottom surface corresponds to $A' = 0$ [Eq. (8a)] and the top surface to $B' = 0$ [Eq. (8b)]. The second top surface corresponds to Eq. (11a) and the second bottom surface to Eq. (11b). Above the bottom surface corresponds to $A' > 0$ and below the bottom surface to $A' < 0$. Above the top surface corresponds to $B' < 0$ and below the top surface to $B' > 0$. Hence the region between these two surfaces corresponds to T1, above the top surface to T2, and below the bottom surface to T3. Below the second bottom surface corresponds to C2 and above the second top surface to C1. The region between these two surfaces corresponds to C3. Note that these four surfaces all meet at a line with $a' = 1$. As we cross the surfaces from above, u_θ and $du_\theta(r)/dr$ are continuously changing from T2 and C1 to T1 and C1 to T1 and C3 to T1 and C2, and finally to T3 and C2, as shown in Fig. 1. Their changing shapes are schematically shown in Fig. 2. Note the complete velocity inversion of u_θ in this process and the fact that, if $\omega_i > 0$, the

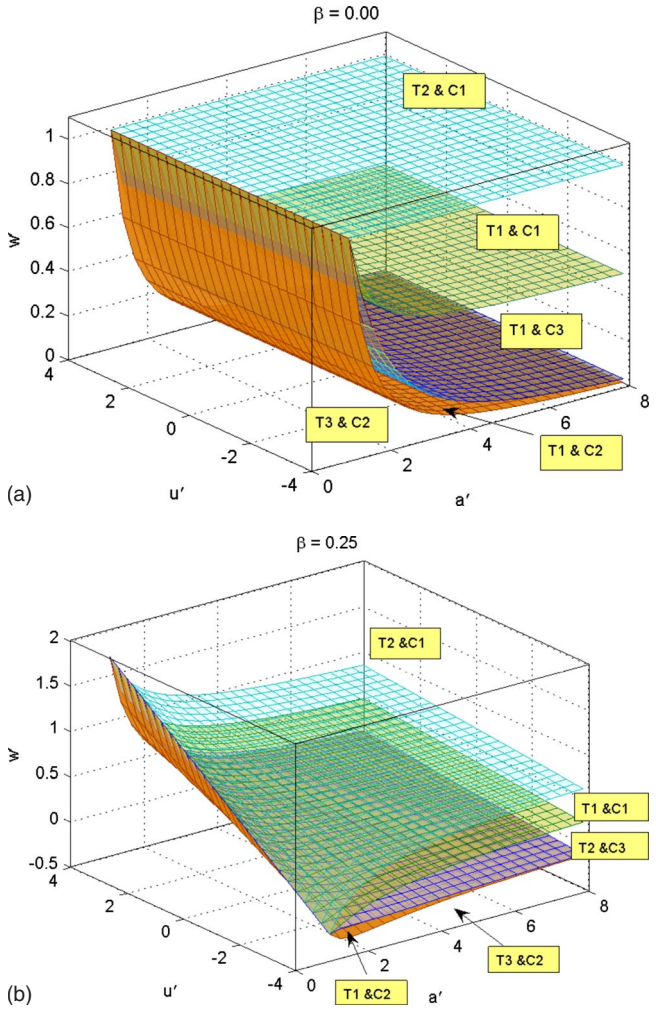

FIG. 1. (Color online) Four surfaces satisfying Eqs. (8) and (11) divide the space into five regions when $\omega_i\omega_o \geq 0$. They all meet at $a'=1$. The symbols in the box are explained in the text; for example, T1 represents type 1 and C1 represents case 1. Note that $\beta=0$ implies $u_i=0$.

velocity inversion can most easily occur when $\omega_o=0$ as seen from Figs. 1 and 2. For case 3, the velocity inversion occurs somewhere between $a_i<\tilde{r}<a_o$ where $\tilde{r}'$ is given by

$$\tilde{r}'^2 = a' \frac{(1-\omega')a' + \beta(u'-a')}{\omega' a'^2 - 1 + \beta(1-u'a')}. \tag{12}$$

Slip velocities can be expressed in terms of slip lengths by incorporating the Maxwell slip model [10–12]:

$$u_i = \zeta_i^p \left(\frac{du_\theta(r)}{dr} - \frac{u_\theta(r)}{r} \right)\Bigg|_{r=a_i} = \zeta_i^p \frac{2B}{a_i^2}, \tag{13a}$$

$$u_o = -\zeta_o^p \left(\frac{du_\theta(r)}{dr} - \frac{u_\theta(r)}{r} \right)\Bigg|_{r=a_o} = -\zeta_o^p \frac{2B}{a_o^2}, \tag{13b}$$

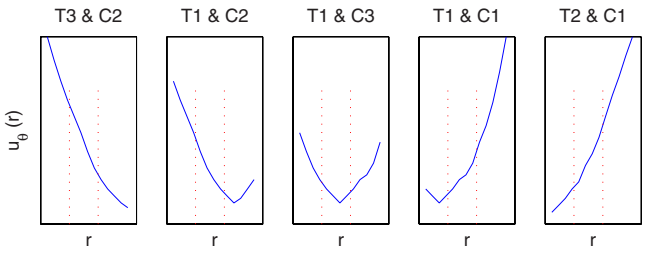

FIG. 2. (Color online) Schematic diagram of $u_\theta(r)$ profiles. The two vertical lines indicate the locations of the inner and the outer walls, respectively. Thus we in fact observe the flow between these two lines. The flow shapes change continuously in turn with the slip conditions at the walls. T3 and C2 can be denoted as normal I, T1 and C2 as normal II, T1 and C3 as partially inverted, T1 and C1 as fully inverted II, and T2 and C1 as fully inverted I.

where ζ^p is the slip length for a flat surface. The slip length for a curved surface with a curvature radius R is given by [7]

$$\frac{1}{\zeta} = \frac{1}{\zeta^p} - \frac{1}{R}. \tag{14}$$

Note that $R>0$ for a convex surface and $R<0$ for a concave surface. We then get the slip lengths at inner and outer walls,

$$\zeta_i = \frac{\zeta_i^p a_i}{a_i - \zeta_i^p}, \quad \zeta_o = \frac{\zeta_o^p a_o}{a_o + \zeta_o^p}. \tag{15}$$

III. SIMULATION RESULTS

The slip velocities cannot be determined in our theoretical considerations. The lack of sufficient knowledge of actual behavior of fluids near the wall makes it difficult to precisely determine them so we have to resort to other methods. Here we will adopt MD to calculate the slip velocities.

Now let us briefly describe the simulation method. All the particles were modeled to move under the modified Lennard-Jones (LJ) potential, given by

$$V_{ij}(r) = 4\epsilon[(r/\sigma)^{-12} - \alpha_{ij}(r/\sigma)^{-6}], \tag{16}$$

where ϵ and σ represent, respectively, standard energy and length parameter, and α_{ij} is a dimensionless parameter to control the attraction between two interacting species. The potential with $\alpha=1$ is the standard LJ potential while the potential with $\alpha=0$ has only a repulsive component. Hereafter all the quantities will be expressed in the LJ reduced unit. The inner wall is rotated with $\omega_i=0.5$ and outer wall is stationary in space with $\omega_o=0$, as suggested from the previous theoretical result. The radius of the inner wall is $a_i=2.05$ and the outer one is $a_o=10.26$. Thus $w'=0$ and $a'=5.01$. The values of β and u' can be actually determined through simulations. The walls themselves are modeled as composed of vibrating solid atoms. The number density of the fluid is set at $\rho=0.4$. The total number of particles is $N=32\,138$. The number of fluid particles (species 1) is 12 361. The number of particles composing the inner wall (species 2) is 1437 and

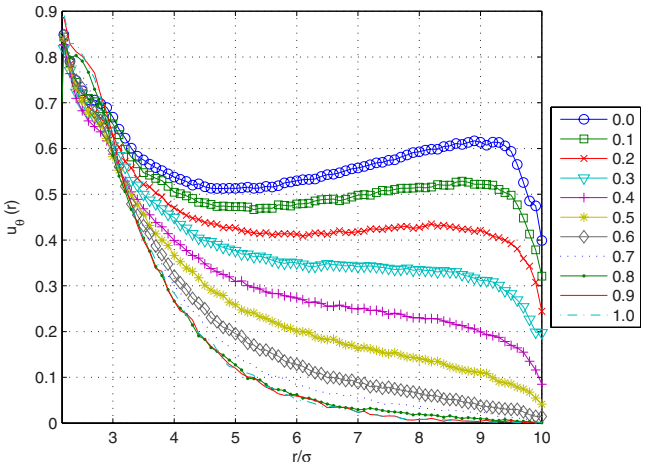

FIG. 3. (Color online) Simulation results of $u_\theta(r)$ profiles with different values of α.

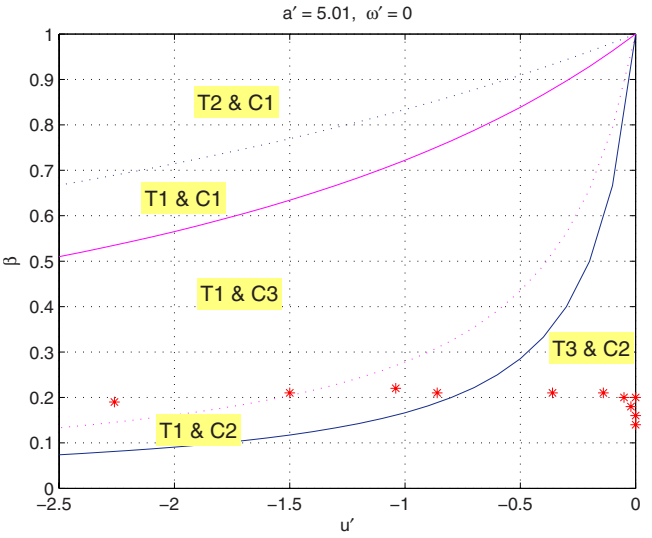

FIG. 4. (Color online) 2D plot of β vs u' as classified according to the values of u_θ and du_θ/dr with $a'=5.01$ and $w'=0$. The simulation results in Table II for 11 different α values are represented by starred points.

the number of particles composing the outer wall (species 3) is 18 340. Attraction parameters α_{ij} between species i and j are set as follows: $\alpha_{11}=\alpha_{12}=1.0$, and the value of α_{13} between the fluid and outer wall is allowed to vary from 0.0 to 1.0 in order to control slip velocities. The temperature of the system is increased with time due to the rotation of the inner wall. Thus the fluid temperature is controlled by the Langevin thermostat to set the temperature at $T=1.0$. We performed MD simulations by using the LAMMPS [14] package with some modifications or additions necessary for simulating our cylindrical Couette flow.

Now we will focus on the calculation of slip velocities at two walls to determine the four variables mentioned in the previous section. The tangential velocity profiles for different values of α are shown in Fig. 3. These results are quite compatible to Ref. [13] if taken into account the fact that a_o and ω_i are different. For $\alpha \leq 0.2$ we can clearly see the velocity inversion. The slip velocities u_i and u_o can be directly estimated from Fig. 3. All the other values are calculated by using the previous theoretical equations. The detailed simulated results are summarized in Table II.

To examine the velocity inversion in another way, we draw a two-dimensional (2D) plot of β vs u' with $w'=0$ and $a'=5.01$ in Fig. 4. As can be seen from Table II, u_θ shows to have type 1 when $\alpha \leq 0.3$ and type 3 otherwise. This fact can also be confirmed in Fig. 4: the four points with $\alpha \leq 0.3$ are located between the two lines just above the bottom (T1) line. From Table II, du_θ/dr also is shown to have case 3 when $\alpha \leq 0.1$ and case 2 otherwise. Thus the two points with $\alpha \leq 0.1$ are located between the two lines just above the second bottom (T1 and C3, partially inverted) line, which can be confirmed in Figs. 3 and 4. In this case it means that there exists a point $\tilde{r}$ of velocity inversion in $a_i < r < a_o$. The point $\tilde{r}_{\text{th}}$ is theoretically calculated by Eq. (12). The point $\tilde{r}_{\text{sim}}$ is

TABLE II. MD simulation data. The attraction parameter α between fluid and outer wall is varied from 0.0 to 1.0. u_i and u_o are the slip velocities at the inner and the outer walls, respectively. They are estimated from Fig. 3. A' and B' are given in Eq. (7). ζ_i and ζ_o are slip lengths at inner and outer walls, respectively, given by Eqs. (13)–(15).

α	u_i	u_o	β	u'	A'	B'	ζ_i	ζ_o
0.0	0.19	−0.43	0.19	−2.26	0.053	0.76	1.91	4.41
0.1	0.22	−0.33	0.21	−1.50	0.034	0.75	1.99	4.17
0.2	0.23	−0.24	0.22	−1.04	0.016	0.76	1.93	3.87
0.3	0.22	−0.19	0.21	−0.86	0.006	0.78	1.79	3.67
0.4	0.22	−0.08	0.21	−0.36	−0.016	0.80	1.66	2.66
0.5	0.22	−0.03	0.21	−0.14	−0.027	0.81	1.60	1.48
0.6	0.20	−0.01	0.20	−0.05	−0.032	0.84	1.49	0.65
0.7	0.18	−0.00	0.18	−0.02	−0.034	0.86	1.40	0.23
0.8	0.20	−0.00	0.20	−0.00	−0.034	0.84	1.48	0.00
0.9	0.16	−0.00	0.16	−0.00	−0.035	0.88	1.32	0.00
1.0	0.14	−0.00	0.14	−0.00	−0.036	0.90	1.25	0.00

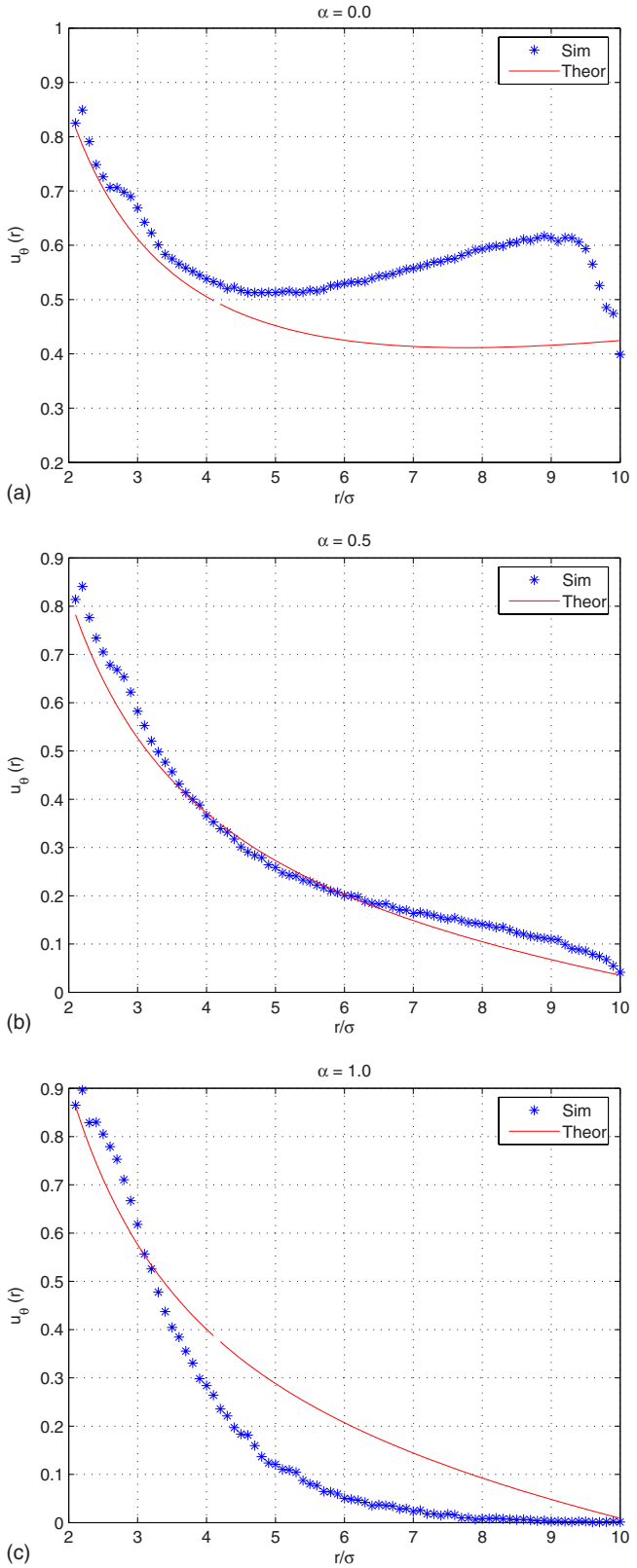

FIG. 5. (Color online) Comparisons of theoretical and simulation results for tangential velocity profiles $u_\theta(r)$. Only 3 out of 11 different values of α in Fig. 3 are shown.

estimated by the simulated data from Fig. 3. The comparison of the two results is rather qualitative, not quantitative; $\tilde{r}_{\mathrm{th}} \approx 7.7$ and $\tilde{r}_{\mathrm{sim}} \approx 5.0$ for $\alpha=0.0$, and $\tilde{r}_{\mathrm{th}} \approx 9.5$ and $\tilde{r}_{\mathrm{sim}} \approx 5.7$ for $\alpha=0.1$.

Let us now compare the theoretical results with simulation results for three different choices of α as shown in Fig. 5. For an intermediate value of $\alpha \approx 0.5$, the two results are comparable. But some small discrepancies still exist near both walls. In the other two cases, the macroscopic NS equation explains well to some extent that near the inner wall they are nearly coincident but near the outer wall they are quite different. For a smaller value of $\alpha \approx 0.0$, they become quite different above from $r \approx 4.5\sigma$ with the theoretical prediction underestimated. For a larger value of $\alpha \approx 1.0$, they are quite different above from $r \approx 3\sigma$ with the theoretical prediction overestimated. Near the inner wall in all cases, overshooting of simulation results over theoretical calculations occurs. In particular, around $r \approx 2.5\sigma$ at $\alpha=0.0$, a small shoulder appears. This manifests the validity limit of the macroscopic equation. This shoulder is smeared out as $\alpha \rightarrow 1.0$. We still do not know why this shoulder appears. Furthermore, near the outer wall, overshooting of simulation results over theoretical calculations becomes reversed at $\alpha = 0.5$ and a large undershooting of simulation results over theoretical calculations appears at $\alpha=1.0$. We must take these discrepancies to be a failure of continuum description.

IV. CONCLUSION

Let us now conclude our results. By employing general slip boundary conditions and the NS equation for a cylindrical Couette flow, we get the tangential velocity profile u_θ expressed with the constants A' and B' in four independent variables of β, slip velocity ratio u', radius ratio a', and angular velocity ratio ω'. By plotting the equations for $A' = 0$ and $B' = 0$, we classify the flows and explore the condition for velocity inversion in the whole space of these four-dimensional variables and find the fact that stationary outer wall gives the best condition for velocity inversion. The constitutive relations such as the slip velocities are calculated with MD simulations. The slip velocities are easily controlled by the attraction parameter α in the generalized LJ potential. The calculated points of velocity inversion are compared with the simulated results. We find that in the intermediate range of the attraction parameter of $\alpha \approx 0.5$ the two results are quite comparable. But at both extreme values of the attraction parameter they are quite different. In any way, the fact that the macroscopic description employing the NS equation can explain the nanoscale behaviors to some extent rather well is quite surprising. The combination of the NS equation and MD simulation can be very effective in explaining the behavior of slip velocity and velocity inversion. More MD simulations should be followed at different thermodynamic states and simulation control parameters for further confirmation.

[1] J. Koplik and J. Banavar, Annu. Rev. Fluid Mech. **27**, 257 (1995).
[2] S. Garimella and C. Sobvan, Annu. Rev. Heat Transfer **13**, 1 (2003).
[3] Z. Zhang, *Nano/Microscale Heat Transfer* (McGraw-Hill, New York, 2007).
[4] C. Ho and Y. Tai, Annu. Rev. Fluid Mech. **30**, 579 (1998).
[5] H. Bruus, *Theoretical Microfluidics* (Oxford University Press, Oxford, 2008).
[6] S. Yuan, *Foundations of Fluid Mechanics* (Prentice Hall, London, 1970); D. Tritton, *Physical Fluid Dynamics* (Oxford University Press, Oxford, 1988).
[7] D. Einzel, P. Panzer, and M. Liu, Phys. Rev. Lett. **64**, 2269 (1990).
[8] K. W. Tibbs, F. Baras, and A. L. Garcia, Phys. Rev. E **56**, 2282 (1997).
[9] K. Aoki, H. Yoshida, T. Nakanishi, and A. L. Garcia, Phys. Rev. E **68**, 016302 (2003).
[10] Y. Sun, R. Barber, and D. Emerson, Proceedings of the 24th International Symposium On Rarefied Gas Dynamics (RGD24, Italy, 2004), AIP Conf. Proc. **762**, 707 (2005); R. Barber, Y. Sun, X. Gu, and D. Emerson, Vacuum **76**, 73 (2004).
[11] S. Yuhong, R. Barber, and D. Emerson, Phys. Fluids **17**, 047102 (2005).
[12] R. Myong, J. Reese, R. Barber and D. Emerson, Phys. Fluids **17**, 087105 (2005).
[13] Y. Jung, Phys. Rev. E **75**, 051203 (2007).
[14] S. Plimpton, J. Comput. Phys. **117**, 1 (1995) http://lammps.sandia.gov.